RESEARCH ARTICLE

Analysis of the Cardiovascular System and an Aorta with Abdominal Aneurysm Using Lattice Boltzmann

Matheus dos Santos Farias[1,*]

[1] University of São Paulo (USP), São Paulo 05508-220, Brazil

Abstract

This study presents a mathematical and computational analysis of blood flow in the abdominal aorta under healthy, aneurysmal, and rupture-related conditions. The proposed framework combines a Newtonian fluid approximation with a Lattice Boltzmann formulation to simulate the hemodynamic behavior of the aorta in three-dimensional geometry. The governing equations were implemented in Python, allowing the generation of numerical simulations and corresponding three-dimensional visualizations of aneurysm progression. The analysis considered clinically inspired stages ranging from the healthy vessel to advanced aneurysmal dilation and rupture. The results showed that aneurysm growth significantly alters the internal flow field, producing changes in velocity distribution, pressure loading, and wall shear stress. As the aneurysmal sac enlarges, the simulations indicate greater hemodynamic disturbance, more pronounced local stress concentration, and reduced structural stability of the aortic wall. In the rupture-related stage, the numerical model captured the transition from confined flow to loss of wall integrity, highlighting the biomechanical severity of advanced aneurysmal disease. From a physical and clinical perspective, the findings reinforce the importance of combining geometry, fluid mechanics, and wall response in the study of abdominal aortic aneurysms. The proposed approach contributes to the interpretation of aneurysm development and rupture risk by linking mathematical modeling to clinically meaningful scenarios. In addition, the work demonstrates the potential of computational methods as support tools for cardiovascular analysis, with relevant applications in bioengineering, biomathematics, and medical modeling. Thus, this study offers an interpretable and innovative framework for investigating the progression of abdominal aortic aneurysms and their hemodynamic consequences.

Keywords: abdominal aortic aneurysm, Lattice Boltzmann method, hemodynamics, Newtonian fluid, computational bioengineering.

1 Introduction

The dynamics of blood flow in arteries is a crucial topic in bioengineering, particularly in the study of pathologies such as aneurysms. An aneurysm is characterized by an abnormal dilation of a blood vessel, usually caused by weakening of the arterial wall.

Submitted: 11 March 2026
Accepted: 30 March 2026
Published: 01 April 2026

Vol. 2, **No.** 2, 2026.
10.62762/JAM.2026.170486

***Corresponding author:**
✉ Matheus dos Santos Farias
matheusfariasfm@gmail.com

Citation
Farias, M. d. S. (2026). Analysis of the Cardiovascular System and an Aorta with Abdominal Aneurysm Using Lattice Boltzmann. *ICCK Journal of Applied Mathematics*, 2(2), 120–136.

This condition may progress to severe complications, including fatal hemorrhage in the event of rupture. According to [1, 2], understanding hemodynamic phenomena is essential for assessing the growth and rupture risk of aneurysms, especially abdominal aneurysms. Early detection and proper monitoring are therefore fundamental for effective treatment, since aneurysms often develop in the aorta, the main artery of the circulatory system, which is continuously subjected to high pressure. As highlighted by [3, 4], this excessive pressure may further aggravate the fragility of the arterial wall, leading to progressive dilation.

This process compromises the normal function of the artery and increases the risk of complications such as obstruction, clot formation, and rupture. A ruptured aneurysm represents a serious medical emergency that may lead to hemorrhagic shock and an imminent risk of death. To prevent such outcomes, imaging techniques such as ultrasound, computed tomography, and magnetic resonance imaging are widely used for the early identification of these dilations. However, according to [5, 6], the challenges involved in analyzing these images have encouraged the use of computational models, such as Computational Fluid Dynamics (CFD), which provide a deeper understanding of hemodynamic behavior and contribute significantly to the clinical management of the disease. Recent clinical evidence also suggests that antiplatelet therapy in AAA patients without symptomatic atherosclerotic disease shows limited benefit in reducing ischemic events while carrying potential bleeding risks [25].

An aneurysm is an abnormal dilation of an artery, often occurring in the aorta because of its large diameter and exposure to high pressure. Abdominal aortic aneurysms (AAA) and thoracic aortic aneurysms (TAA) are particularly critical, as their rupture may result in sudden death [1, 7]. Their prevalence increases with age and is higher among men, smokers, and individuals with hypertension [1, 8]. These alterations affect hemodynamics by modifying blood pressure and shear stress, thereby increasing the risk of severe complications [2, 6]. Aneurysmal dilation also changes blood flow patterns, reducing flow velocity, promoting vortex formation, and favoring thrombus development, all of which contribute to a higher risk of rupture [3, 4]. Understanding these changes is essential for improving diagnosis and treatment. The Lattice Boltzmann Method [9] enables the simulation of complex geometries and allows the analysis of how aneurysm shape and size influence arterial pressure and wall stress. In this study, the model is applied to investigate blood-flow dynamics in aortas affected by aneurysms, providing relevant information for diagnosis and treatment and contributing to advances in personalized medicine. Figure 1 illustrates the characteristic dilation of an aortic aneurysm.

The main objective of this study is to analyze blood-flow dynamics in an abdominal aorta with aneurysmal dilation using the Lattice Boltzmann Method (LBM), which is widely recognized for its efficiency and accuracy in the simulation of complex flows in irregular geometries [9, 10]. The study focuses on the evaluation of hemodynamic quantities such as internal pressure, wall shear stress, and the influence of aneurysm geometry on flow behavior [3, 4, 6]. In addition, the LBM equations were implemented in Python to perform the numerical simulations and generate the corresponding three-dimensional visualizations. The central aim is to investigate the pressure conditions sustained by the aortic wall in the presence of an abdominal aneurysm and to identify critical conditions associated with rupture risk.

The growing number of aortic aneurysm cases, together with their frequently asymptomatic progression until rupture, highlights the need for more detailed studies and more effective methods for diagnosis and treatment [1, 7, 8, 11]. Although previous studies have addressed aortic geometry and structural alterations, there is still a need for computational approaches that combine three-dimensional aneurysm representation with numerical blood-flow simulation and physically interpretable pressure analysis. This gap motivated the present work. Based on established mathematical models, this study applies the Lattice Boltzmann Method to simulate blood flow in a three-dimensional abdominal aortic aneurysm model, using Python as the implementation tool. The proposed approach aims to improve the understanding of the interaction between flow behavior, vessel geometry, and wall loading, with emphasis on conditions that may lead to rupture [5, 21–23]. Machine learning techniques have also been applied to explore the relationship between geometric shape features and numerically predicted rupture risk in aortic aneurysms [27].

2 Literature Review

This section presents the mathematical background of the main concepts involved in the present study, including the circulatory system, blood

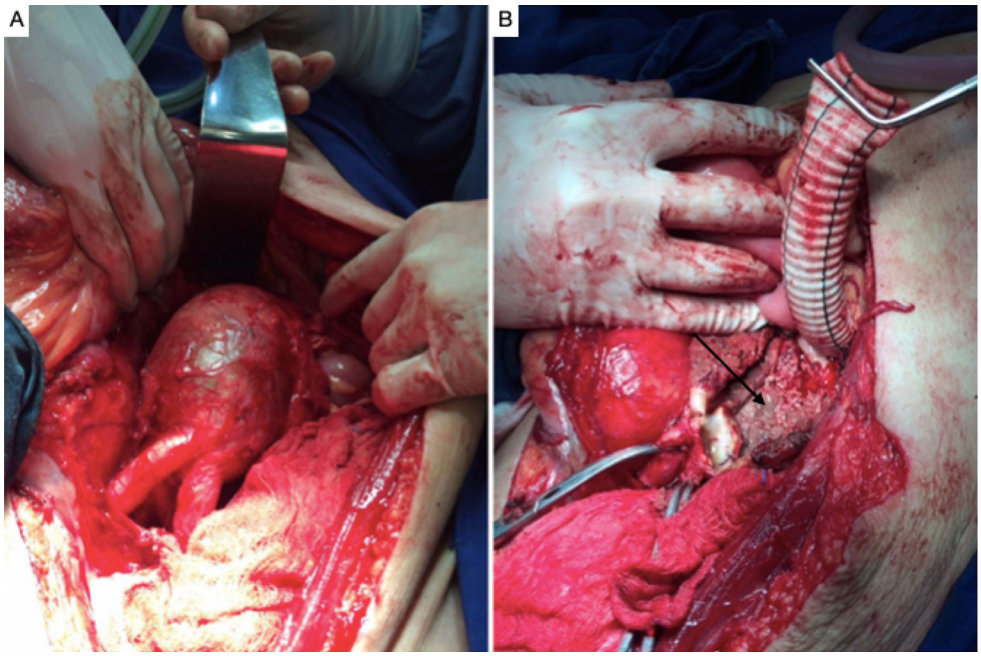

Figure 1. Example of an aortic aneurysm.
Source: Adapted from article available at: https://www.scielo.br/j/jvb/a/zrWb3pLtpHWQKJjzRGS9vKP/?lang=pt

rheology, and Newtonian and non-Newtonian fluid models. Although different rheological models are discussed for theoretical completeness, the numerical simulations performed in this work adopt a **Newtonian fluid approximation** for blood flow in the abdominal aorta. This choice is appropriate for large arteries, where blood can often be reasonably modeled with constant viscosity.

2.1 Circulatory System

The circulatory system is responsible for transporting oxygen, nutrients, hormones, and metabolic waste throughout the body. It is composed of the heart, the blood vessels, and the blood itself [1]. From a mathematical point of view, simplified dynamical models can be used to describe the interaction between flow-related variables, pressure, and vascular response, as follows:

$$\frac{dI}{dt} = \alpha I - \beta IP \tag{1}$$

$$\frac{dP}{dt} = \gamma P - \delta PI \tag{2}$$

$$\frac{dA}{dt} = \epsilon I - \zeta A \tag{3}$$

In these equations, I represents a flow-related quantity, P denotes pressure, and A represents a vascular area-related parameter. The coefficients α, β, γ, δ, ϵ, and ζ describe the interaction and evolution of these variables. Physically, this system expresses how blood flow, pressure, and vascular geometry may vary together in a simplified cardiovascular framework, which is consistent with the hemodynamic focus of the present study.

2.2 Rheology

Rheology is the branch of mechanics that studies the deformation and flow of materials under applied forces [12]. In the context of blood flow, rheology is important because it describes how blood responds to stress and deformation inside the vessel. A basic constitutive relation may be written as

$$\sigma_{ij} = E\,\epsilon_{ij}, \quad i,j = x,y,z \tag{4}$$

where σ_{ij} is the stress tensor, E is the elastic modulus, and ϵ_{ij} is the strain tensor. In physical terms, this equation relates the internal mechanical response of a material to its deformation. In the present work, this concept is relevant because the pressure exerted by blood flow is associated with the mechanical loading experienced by the aortic wall.

Although this class of models is important in blood rheology, it is not the model adopted in the present simulations. Fluid-structure interaction (FSI) effects, including the influence of haematocrit on wall

dynamics in abdominal aortic aneurysms, have also been investigated in previous studies [24].

2.3 Newtonian Fluid

A Newtonian fluid is characterized by constant viscosity and a linear relationship between shear stress and shear rate. This relation is given by

$$\tau = \eta\dot{\gamma} \tag{5}$$

where τ is the shear stress, η is the dynamic viscosity, and $\dot{\gamma}$ is the shear rate. Physically, this means that the resistance to flow remains proportional to the rate of deformation. In this study, this is the rheological model adopted in the simulations, since the abdominal aorta is a large vessel and the constant-viscosity approximation is suitable for the proposed numerical analysis.

2.4 Non-Newtonian Fluid

Non-Newtonian fluids do not have constant viscosity. Instead, their viscosity changes with shear rate or with time, depending on the constitutive model. A common representation is the power-law model [12]:

$$\tau = K\dot{\gamma}^n \tag{6}$$

where K is the consistency index and n is the flow behavior index. When $n < 1$, the fluid exhibits shear-thinning behavior; when $n > 1$, it exhibits shear-thickening behavior. Physically, this equation shows that the apparent resistance to flow is not constant. Although this class of models is important in blood rheology, it is not the model adopted in the present simulations.

2.5 Time-Independent Non-Newtonian Fluids

Time-independent non-Newtonian fluids are those whose viscosity depends only on the instantaneous shear rate. This group includes pseudoplastic, dilatant, Bingham, Herschel–Bulkley, and Casson fluids. These models are relevant in hemodynamic studies because they describe how the apparent viscosity changes under different flow conditions [3, 5, 9]. In physical terms, these models are useful when the fluid behavior changes with the local deformation rate, but not explicitly with time.

2.6 Time-Dependent Non-Newtonian Fluids

Time-dependent non-Newtonian fluids exhibit viscosity that varies with both time and deformation history. A simplified form of this behavior may be written as

$$\eta(t) = \eta_0\,(1 - \alpha t)\,, \quad t \le t_{\max} \tag{7}$$

where η_0 is the initial viscosity, α is a temporal parameter, and $t_{\max}$ is the limiting time for the model validity. Physically, this expression describes materials whose internal structure evolves during flow. This formulation is presented here as theoretical background and is not directly used in the present numerical implementation.

3 Mathematical Modeling

3.1 Mathematical Formulation of the Newtonian Model

In the present study, blood flow in the abdominal aorta is modeled under the incompressible Newtonian hypothesis. Although blood may exhibit non-Newtonian behavior at low shear rates and in small vessels, the Newtonian approximation is widely adopted in large arteries, where the shear rate is relatively high and the effective viscosity can be reasonably approximated as constant [13, 14]. This assumption is particularly useful in abdominal aortic simulations because it allows the analysis to focus on pressure-driven transport, velocity redistribution, aneurysmal expansion, and wall loading without introducing additional rheological complexity that is not essential for the main hemodynamic mechanisms investigated here.

Let $\mathbf{u} = (u_x, u_y, u_z)$ denote the velocity field, p the pressure, ρ the density, and μ the dynamic viscosity. For a Newtonian fluid, the deviatoric stress tensor is linearly related to the rate of deformation tensor. The symmetric strain-rate tensor is defined by

$$\mathbf{D}(\mathbf{u}) = \frac{1}{2}\left(\nabla\mathbf{u} + \nabla\mathbf{u}^T\right), \tag{8}$$

where $\nabla\mathbf{u}$ is the velocity gradient tensor. In component form,

$$D_{ij} = \frac{1}{2}\left(\frac{\partial u_i}{\partial x_j} + \frac{\partial u_j}{\partial x_i}\right), \qquad i,j \in \{1,2,3\}. \tag{9}$$

Physically, $\mathbf{D}(\mathbf{u})$ measures the local rate at which fluid elements deform. In biofluid mechanics, this

tensor is essential because it quantifies how blood changes shape while moving through the aortic lumen, especially near the aneurysmal wall, where strong velocity gradients may develop.

The constitutive law for an incompressible Newtonian fluid is then written as

$$\boldsymbol{\sigma} = -p\mathbf{I} + 2\mu\mathbf{D}(\mathbf{u}), \tag{10}$$

or, equivalently, in components,

$$\sigma_{ij} = -p\,\delta_{ij} + \mu\left(\frac{\partial u_i}{\partial x_j} + \frac{\partial u_j}{\partial x_i}\right), \tag{11}$$

where $\boldsymbol{\sigma}$ is the Cauchy stress tensor, $\mathbf{I}$ is the identity tensor, and δ_{ij} is the Kronecker delta. This expression separates the total stress into an isotropic pressure contribution and a viscous contribution associated with deformation. Physically, it means that blood transmits normal forces through pressure and tangential forces through viscosity. This distinction is important in aneurysm studies because pressure contributes to wall distension, while viscous stresses contribute to wall shear and endothelial loading.

For simple shear flow, Eq. (11) reduces to the familiar scalar relation

$$\tau = \mu\dot{\gamma}, \tag{12}$$

where τ is the shear stress and $\dot{\gamma}$ is the shear rate. Thus, the Newtonian model states that shear stress grows linearly with the rate of deformation. In the abdominal aorta, this relation provides a direct and interpretable connection between blood motion and the viscous forces applied to the vessel wall.

The incompressibility condition is expressed by the continuity equation

$$\nabla \cdot \mathbf{u} = 0. \tag{13}$$

This relation states that the local fluid volume is conserved. In physical terms, blood does not accumulate or disappear inside the computational domain, which is an appropriate assumption for large-vessel hemodynamics under physiological conditions.

The conservation of linear momentum is written as

$$\rho\frac{D\mathbf{u}}{Dt} = \nabla \cdot \boldsymbol{\sigma} + \mathbf{f}, \tag{14}$$

where $\mathbf{f}$ denotes body forces and

$$\frac{D\mathbf{u}}{Dt} = \frac{\partial \mathbf{u}}{\partial t} + (\mathbf{u}\cdot\nabla)\mathbf{u} \tag{15}$$

is the material derivative. Equation (15) expresses the total acceleration experienced by a fluid particle and contains both local temporal variation and convective transport. In the aorta, the convective term becomes especially relevant in enlarged regions, where the aneurysmal geometry alters the spatial distribution of velocity and may promote recirculation.

Substituting Eq. (10) into Eq. (14), one obtains

$$\rho\frac{D\mathbf{u}}{Dt} = -\nabla p + \nabla \cdot (2\mu\mathbf{D}(\mathbf{u})) + \mathbf{f}. \tag{16}$$

If μ is constant and the flow is incompressible, then

$$\nabla \cdot (2\mu\mathbf{D}(\mathbf{u})) = \mu\nabla^2\mathbf{u}, \tag{17}$$

and Eq. (16) reduces to the incompressible Navier–Stokes equation:

$$\rho\left(\frac{\partial \mathbf{u}}{\partial t} + \mathbf{u}\cdot\nabla\mathbf{u}\right) = -\nabla p + \mu\nabla^2\mathbf{u} + \mathbf{f}. \tag{18}$$

This derivation shows why the Newtonian model is mathematically convenient and physically relevant for the present problem. It yields a closed system composed of Eqs. (13) and (18), in which pressure, inertia, and viscosity interact directly with the aneurysmal geometry. In applied hemodynamics, these equations govern the redistribution of blood velocity, the formation of disturbed-flow regions, and the increase in wall loading as the vessel dilates.

To further interpret the model, it is useful to nondimensionalize the equations. Let U be a characteristic velocity, L a characteristic length, and $P_0 = \rho U^2$ a characteristic pressure. Define the dimensionless variables

$$\mathbf{x}^* = \frac{\mathbf{x}}{L}, \qquad t^* = \frac{tU}{L}, \qquad \mathbf{u}^* = \frac{\mathbf{u}}{U}, \qquad p^* = \frac{p}{\rho U^2}. \tag{19}$$

Substituting Eq. (19) into Eq. (18) yields

$$\frac{\partial \mathbf{u}^*}{\partial t^*} + \mathbf{u}^* \cdot \nabla^* \mathbf{u}^* = -\nabla^* p^* + \frac{1}{Re} \nabla^{*2} \mathbf{u}^* + \mathbf{f}^*, \tag{20}$$

where

$$Re = \frac{\rho U L}{\mu} \tag{21}$$

is the Reynolds number. The Reynolds number measures the ratio of inertial to viscous effects. In abdominal aortic flow, it provides a concise criterion for understanding whether the local hemodynamics are dominated by viscous damping or by inertial transport. As aneurysmal dilation increases the characteristic length L, the local flow may become more disturbed, and this may amplify recirculation and stress redistribution even without turbulence.

Under pulsatile conditions, another relevant dimensionless parameter is the Womersley number,

$$\alpha = R\sqrt{\frac{\omega \rho}{\mu}}, \tag{22}$$

where R is the vessel radius and ω is the angular frequency of pulsation. This quantity compares transient inertial effects with viscous diffusion across the vessel radius. In large arteries such as the aorta, α is not negligible, meaning that pulsatility strongly influences the velocity profile and the temporal distribution of wall shear stress.

For fully developed steady Newtonian flow in a straight cylindrical vessel, the axial momentum equation simplifies to

$$\mu \left(\frac{1}{r} \frac{d}{dr} \left(r \frac{du}{dr} \right) \right) = \frac{dp}{dz}, \tag{23}$$

where $u = u(r)$ is the axial velocity and dp/dz is the axial pressure gradient. Integrating Eq. (23) under no-slip conditions gives the parabolic profile

$$u(r) = -\frac{1}{4\mu} \frac{dp}{dz} \left(R^2 - r^2 \right). \tag{24}$$

The corresponding volumetric flow rate is

$$Q = \int_0^R 2\pi r \, u(r) \, dr = -\frac{\pi R^4}{8\mu} \frac{dp}{dz}, \tag{25}$$

which leads to the classical pressure–flow relation

$$\Delta p = \frac{8\mu L Q}{\pi R^4}. \tag{26}$$

Although aneurysmal flow is not fully developed and the geometry is not cylindrical, Eqs. (24)–(26) remain useful as analytical references. They show that pressure loss depends strongly on vessel radius, and thus highlight how geometric changes can dramatically alter flow resistance. In aneurysms, however, the enlarged sac disrupts this simple behavior and introduces secondary flow structures and local stagnation zones.

A relevant wall quantity in vascular mechanics is the wall shear stress (WSS), defined by

$$\tau_w = \mu \left. \frac{\partial u_t}{\partial n} \right|_{\text{wall}}, \tag{27}$$

where u_t is the tangential velocity component and n is the outward wall-normal direction. This quantity measures the tangential friction exerted by blood on the endothelium. In aneurysm studies, WSS is especially important because regions of abnormally low or spatially heterogeneous WSS are associated with disturbed flow, endothelial dysfunction, thrombus-related processes, and wall remodeling.

For pulsatile flow, time-averaged and oscillatory indicators are often used. The time-averaged wall shear stress (TAWSS) is

$$\text{TAWSS} = \frac{1}{T} \int_0^T |\tau_w(t)| \, dt, \tag{28}$$

and the oscillatory shear index (OSI) is defined as

$$\text{OSI} = \frac{1}{2} \left(1 - \frac{\left| \int_0^T \tau_w(t) \, dt \right|}{\int_0^T |\tau_w(t)| \, dt} \right). \tag{29}$$

Here, T is the cardiac-cycle period. TAWSS quantifies the average magnitude of shear loading over one cycle, whereas OSI measures directional oscillation of the wall shear vector. In physical terms, high OSI indicates strongly reversing or disturbed near-wall flow, which is often observed inside aneurysmal sacs and is relevant to vascular degeneration.

The pressure loading acting on the wall is classically related to vessel geometry by Laplace's law. In simplified cylindrical form,

$$\sigma_\theta = \frac{pr}{h}, \tag{30}$$

where σ_θ is the circumferential wall stress, p is the internal pressure, r is the local radius, and h is the wall thickness. This equation shows that larger radius and higher pressure produce greater circumferential stress, whereas greater wall thickness reduces it. In the abdominal aortic aneurysm, the local increase in r and the progressive reduction in h both act in the same direction, increasing the likelihood of wall failure. Earlier fluid-structure interaction studies have examined the effects of asymmetry and wall thickness on hemodynamics in abdominal aortic aneurysms [28].

To relate hemodynamic loading to wall deformation, a simplified linear elastic relation may be adopted:

$$\sigma = E\epsilon, \tag{31}$$

where σ is stress, E is the elastic modulus, and ϵ is strain. Equation (31) states that deformation is proportional to loading, with the proportionality controlled by wall stiffness. Although the present study focuses on fluid flow rather than full fluid–structure interaction, this relation is useful for interpreting how pressure-induced wall stress may translate into distension, loss of stability, and eventual rupture.

Combining Eqs. (30) and (31), one obtains the approximate strain estimate

$$\epsilon \approx \frac{pr}{Eh}, \tag{32}$$

which explicitly links pressure, radius, wall thickness, and stiffness. This relation is particularly meaningful in aneurysm analysis because it shows that larger aneurysms are not dangerous only because they are larger geometrically, but because their geometry amplifies wall strain for the same pressure level.

Therefore, the Newtonian formulation adopted in this work is mathematically robust, physically interpretable, and well suited to the simulation of abdominal aortic flow. It provides a closed framework in which mass conservation, momentum balance, viscous stresses, pulsatile hemodynamic indicators, and simplified wall mechanics can be analyzed consistently. This is precisely why the Newtonian approximation is important in the present simulations: it captures the dominant large-artery flow mechanisms while preserving enough mathematical structure to interpret pressure redistribution, wall shear stress, aneurysmal growth, and rupture-related loading in a clear bioengineering context.

3.2 Boltzmann Equations

The Lattice Boltzmann Method (LBM) is a numerical approach derived from the Boltzmann equation and is widely used to simulate fluid flow in complex geometries [9, 10]. In the present study, the method is employed to simulate blood flow in a **three-dimensional** aortic geometry under three conditions: a healthy aorta, an abdominal aortic aneurysm, and a ruptured aneurysm configuration. The main objective is to evaluate how pressure, velocity, and wall-loading conditions change as the geometry evolves.

The continuous Boltzmann equation is written as

$$\frac{\partial f(\mathbf{x},\mathbf{v},t)}{\partial t} + \mathbf{v}\cdot\nabla f(\mathbf{x},\mathbf{v},t) = \Omega\big(f(\mathbf{x},\mathbf{v},t)\big), \tag{33}$$

where $f(\mathbf{x},\mathbf{v},t)$ is the particle distribution function, $\mathbf{x}$ is the spatial position, $\mathbf{v}$ is the particle velocity, and $\Omega(f)$ is the collision operator. Physically, this equation describes the evolution of particle populations in space and time due to transport and collisions. In the present work, this formulation provides the mathematical basis for representing blood flow in the aortic domain.

To simplify the collision term, the BGK (Bhatnagar–Gross–Krook) approximation is adopted [9]:

$$\Omega(f) = -\frac{1}{\tau}\left(f(\mathbf{x},\mathbf{v},t) - f_{\text{eq}}(\mathbf{x},\mathbf{v},t)\right), \tag{34}$$

where τ is the relaxation time and f_{eq} is the equilibrium distribution function. The parameter τ is directly related to viscous effects in the fluid. Physically, this equation states that the distribution function tends to relax toward local equilibrium after collisions, which is consistent with the dissipative nature of blood flow.

For numerical implementation, the Boltzmann equation is discretized in space, time, and velocity. Since the present work considers a **three-dimensional** geometry, the LBM formulation is written in a discrete 3D lattice form as

$$f_i(\mathbf{x}+\mathbf{c}_i\Delta t, t+\Delta t) = f_i(\mathbf{x},t) - \frac{1}{\tau}\left[f_i(\mathbf{x},t) - f_{\text{eq},i}(\mathbf{x},t)\right], \tag{35}$$

where f_i is the discrete distribution function associated with the lattice direction i, $\mathbf{c}_i$ is the discrete lattice velocity, and $f_{\text{eq},i}$ is the corresponding equilibrium distribution. Physically, this equation combines two processes at each time step: particle propagation through the computational lattice and relaxation toward equilibrium. In the present application, this evolution makes it possible to simulate blood-flow patterns inside the aorta and to identify regions affected by aneurysmal dilation.

3.3 Application of LBM to Blood Flow in the Aorta

In this study, the LBM is applied to simulate blood flow in three different aortic conditions: a healthy geometry, an abdominal aortic aneurysm, and a rupture-related configuration. This comparison allows the analysis of how geometric changes influence the internal pressure field, the velocity distribution, and the mechanical loading associated with rupture risk [3–5]. The numerical implementation was performed in Python, and the results were post-processed to obtain three-dimensional visualizations of the simulated aortic flow. Advanced modeling approaches, such as transmission line models used as digital twins, offer promising non-invasive methods for personalized monitoring of abdominal aortic aneurysm progression and post-repair hemodynamics [26].

The equilibrium distribution function is written as

$$f_{\text{eq},i} = w_i\rho\left[1 + \frac{\mathbf{c}_i\cdot\mathbf{u}}{c_s^2} + \frac{(\mathbf{c}_i\cdot\mathbf{u})^2}{2c_s^4} - \frac{\mathbf{u}\cdot\mathbf{u}}{2c_s^2}\right], \tag{36}$$

where w_i are the lattice weights, ρ is the fluid density, $\mathbf{u}$ is the macroscopic velocity, and c_s is the lattice speed of sound. This expression defines the local equilibrium state toward which the distribution functions relax during the collision step. Physically, it connects the microscopic lattice representation to macroscopic flow quantities, allowing the model to reproduce the main hemodynamic features of blood flow.

The numerical solution also requires appropriate boundary conditions. In the present model, the aortic wall is represented using a no-slip bounce-back condition, while inlet and outlet conditions are imposed to control the flow entering and leaving the computational domain [9, 10]. These conditions can be summarized as follows:

- **Wall condition**: a bounce-back scheme is used to represent the aortic wall, enforcing zero normal flow through the wall and reproducing the no-slip condition.
- **Inlet and outlet conditions**: prescribed flow or velocity conditions are imposed at the ends of the aortic segment in order to simulate different hemodynamic states, including pressure increase and aneurysmal dilation.

Physically, these boundary conditions are essential because they define how blood interacts with the vessel wall and how the flow enters and leaves the aortic segment. This is particularly important in aneurysm simulations, where wall confinement and flow recirculation strongly influence pressure redistribution.

After the evolution of the distribution functions, the macroscopic variables are recovered from their discrete moments. The fluid density is obtained from

$$\rho(\mathbf{x},t) = \sum_i f_i(\mathbf{x},t), \tag{37}$$

and the macroscopic velocity is computed as

$$\mathbf{u}(\mathbf{x},t) = \frac{1}{\rho(\mathbf{x},t)}\sum_i \mathbf{c}_i f_i(\mathbf{x},t). \tag{38}$$

Here, $\rho(\mathbf{x},t)$ represents the local fluid density and $\mathbf{u}(\mathbf{x},t)$ represents the local flow velocity. Physically, these quantities describe the hemodynamic state inside

the aorta and are used to evaluate how aneurysm formation alters blood transport, local velocity reduction, and the pressure-related mechanical demand imposed on the vessel wall.

Therefore, the LBM formulation adopted in this work provides a computationally efficient framework for simulating blood flow in three-dimensional aortic geometries. By comparing the healthy, aneurysmal, and rupture-related cases, the model makes it possible to investigate how geometric deterioration affects blood-flow behavior and the pressure conditions associated with wall failure.

Numerical approximation schemes for partial differential equations also play an important role in efficient simulation of complex physical systems relevant to hemodynamic modeling [29].

4 Results and Discussions

4.1 Simulation Cases and Hemodynamic Interpretation

The numerical simulations were implemented in Python using a three-dimensional Lattice Boltzmann framework applied to four representative abdominal aortic configurations: a healthy aorta, an aneurysmal aorta, a high-risk aneurysmal configuration, and a rupture scenario. The clinical and physical parameters adopted in the simulations were selected from the literature on abdominal aortic geometry, blood rheology in large arteries, and abdominal aortic aneurysm risk assessment [13, 15, 17, 18]. In the present work, blood was modeled as an incompressible Newtonian fluid, which is a common approximation for flow in the aorta [13, 14]. The purpose of these four cases is to show the progressive change in hemodynamic loading as the geometry evolves from a normal vessel to aneurysmal dilation and finally to a rupture-related condition.

4.2 Global Physical Parameters Used in the Simulations

The global physical parameters adopted in all simulations are representative of abdominal aortic hemodynamics reported in the literature [13, 14]. These values were used as the common physical basis for the healthy, aneurysmal, high-risk, and rupture-related cases, as summarized in Table 1.

These parameters define the common hemodynamic framework of the simulations. The values of ρ and μ control the inertial and viscous behavior of blood, while the no-slip wall condition ensures a physically consistent interaction between the flow and the vessel wall [13, 14]. Since the study focuses on the abdominal aorta, the Newtonian approximation provides a direct interpretation of pressure, velocity, and wall shear stress distributions.

Table 1. Global physical parameters adopted in the simulations based on the literature [13, 14].

Parameter	Value	Unit / Description
Blood density, ρ	1060	kg/m^3
Dynamic viscosity, μ	0.0035	Pa·s
Fluid model	Newtonian	Constant viscosity approximation
Flow regime	Incompressible	Suitable for large arteries
Wall condition	No-slip / bounce-back	Impermeable aortic wall
Geometry type	3D	Abdominal aorta
Numerical implementation	Python	LBM-based solver

4.3 Case I: Healthy Abdominal Aorta

The first simulation represents a healthy abdominal aorta without aneurysmal dilation. This case is used as the physiological reference configuration against which the pathological cases are compared. The geometric values adopted for this stage were based on normal abdominal aortic dimensions reported in the literature [15], as summarized in Table 2.

Figure 2 presents the three-dimensional simulation of the healthy abdominal aorta, showing the undisturbed flow field characteristic of the physiological state.

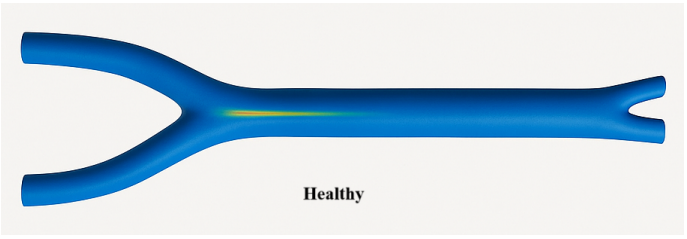

Figure 2. Three-dimensional simulation of the healthy abdominal aorta.

In the healthy configuration, the flow remains guided by the vessel lumen and the hemodynamic field is concentrated along the axial direction. Physically, this indicates organized transport, limited recirculation,

Table 2. Representative parameters for the healthy aortic configuration based on the literature [13, 15].

Parameter	Value	Description
Mean abdominal aortic diameter	17.5	mm
Reference male diameter	18.4	mm
Reference female diameter	15.9	mm
Wall thickness	2.0	mm
Reference systolic pressure	120	mmHg
Reference diastolic pressure	80	mmHg
Mean arterial pressure (approx.)	93.3	mmHg
Structural condition	Intact wall	No aneurysmal bulging
Clinical status	Healthy	Baseline case

and physiological wall loading. Therefore, the healthy case serves as the baseline for interpreting the hemodynamic alterations observed in the aneurysmal and rupture-related stages [14, 15].

4.4 Case II: Abdominal Aortic Aneurysm

The second simulation considers an aneurysmal aorta with localized dilation. In this case, the enlarged lumen modifies the local flow organization, reducing the mean velocity inside the aneurysmal sac and promoting redistribution of pressure and wall loading. The geometric threshold used to characterize this case follows the abdominal aortic aneurysm criteria reported in the literature [15, 16], as summarized in Table 3.

Figure 3 presents the three-dimensional simulation of the abdominal aorta with aneurysmal dilation, illustrating the altered flow patterns within the enlarged sac.

In the aneurysmal configuration, the enlargement of the lumen alters the local velocity field and tends to create a broader low-momentum region inside the sac. Physically, this means that blood transport becomes less uniform, with greater tendency for recirculation and redistribution of wall shear stress. Even before rupture, this altered hemodynamic environment may

Table 3. Representative parameters for the aneurysmal aortic configuration based on the literature [16, 17].

Parameter	Value	Description
Maximum aneurysm diameter	45	mm
AAA diagnostic threshold	≥ 30	mm
Approximate wall thickness	2.0	mm
Representative systolic pressure	130	mmHg
Representative diastolic pressure	85	mmHg
Mean arterial pressure (approx.)	100.0	mmHg
Structural condition	Dilated wall	Local aneurysmal expansion
Clinical status	Non-ruptured AAA	Intermediate-risk case

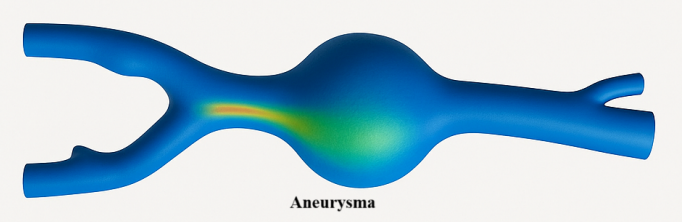

Figure 3. Three-dimensional simulation of the abdominal aorta with aneurysmal dilation.

contribute to progressive wall weakening and further aneurysm growth [17, 18].

4.5 Case III: High-Risk Aneurysmal Configuration

The third simulation represents a more advanced aneurysmal stage, approaching a rupture-prone configuration. This case is interpreted as a high-risk stage characterized by larger diameter, higher pressure loading, and stronger local stress concentration. The adopted dimensions are consistent with clinical repair thresholds and rupture-risk discussion found in the literature [17–19], as summarized in Table 4.

Figure 4 illustrates the three-dimensional high-risk aneurysmal configuration, showing marked wall loading and localized rupture-related outflow.

This stage shows a pronounced concentration of the hemodynamic field near the damaged region. Physically, the increased diameter reduces geometric stability, while the elevated pressure and wall thinning increase local mechanical demand. The warm-color

Table 4. Representative parameters for the high-risk aneurysmal configuration based on the literature [18–20].

Parameter	Value	Description
Maximum aneurysm diameter	55	mm
Classical male repair threshold	55	mm
Classical female repair threshold	50	mm
Dilated-region wall thickness	2.02	mm
Representative systolic pressure	160	mmHg
Representative diastolic pressure	95	mmHg
Mean arterial pressure (approx.)	116.7	mmHg
Structural condition	Marked dilation	High-risk aneurysmal stage
Clinical status	Rupture-prone geometry	Advanced disease stage

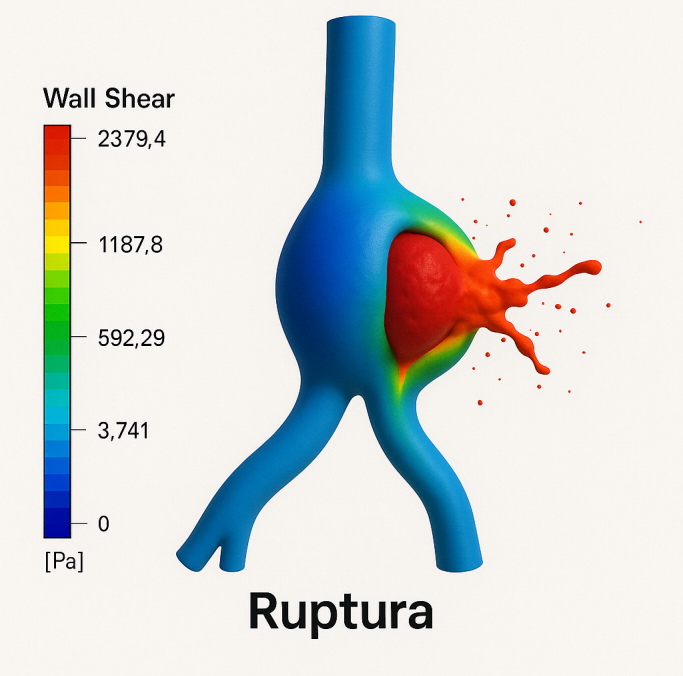

Figure 4. Three-dimensional high-risk aneurysmal configuration showing marked wall loading and localized rupture-related outflow.

region indicates intense hemodynamic loading close to the rupture-prone site, suggesting that the vessel is no longer operating under stable physiological conditions [17, 18].

4.6 Case IV: Rupture Scenario

The fourth simulation represents the rupture scenario, in which structural failure is already present and the flow escapes through the compromised wall region. This case illustrates the extreme hemodynamic condition associated with loss of vessel integrity and severe biomechanical instability [17, 18], as detailed in Table 5.

Table 5. Representative parameters for the rupture scenario based on the literature [17, 18, 20].

Parameter	Value	Description
Maximum local diameter	60–65	mm
Approximate wall thickness	1.5–2.0	mm
Representative systolic pressure	180	mmHg
Representative diastolic pressure	110	mmHg
Mean arterial pressure (approx.)	133.3	mmHg
Wall shear stress scale in the figure	0–2379.4	Pa
Structural condition	Wall failure	Ruptured aneurysm
Clinical status	Rupture scenario	Severe hemodynamic instability

Figure 5 presents the three-dimensional rupture scenario, showing the wall shear stress scale and externalized flow through the failed wall region.

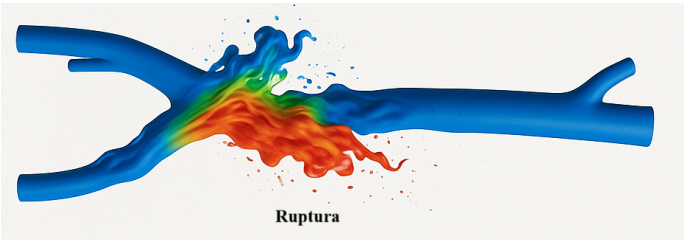

Figure 5. Three-dimensional rupture scenario with wall shear stress scale and externalized flow through the failed wall region.

In the rupture scenario, the flow is no longer confined by the vessel wall, and the simulated field shows a strong localized concentration around the rupture opening. Physically, this indicates a critical loss of structural containment, producing highly abnormal wall shear and pressure redistribution. From

a biomechanical perspective, this stage represents failure of the vessel wall to withstand the imposed hemodynamic load [17, 18].

4.7 General Physical Interpretation of the Four Stages

The sequence of simulations shows a progressive transition from physiological flow to pathological hemodynamics. In the healthy aorta, the vessel geometry supports a stable axial flow [14, 15]. In the aneurysmal case, the enlarged lumen modifies transport and promotes disturbed flow [16, 17]. In the high-risk stage, the combined effect of larger diameter, increased pressure, and wall thinning intensifies local loading [18, 19]. Finally, in the rupture scenario, the vessel wall can no longer contain the blood flow, leading to a mechanically unstable configuration [17]. Therefore, the simulations provide a physically interpretable description of how aneurysm progression changes the internal flow field and increases the likelihood of wall failure.

4.8 Progressive Clinical Simulations of Abdominal Aortic Aneurysm

4.8.1 Simulation Parameters and Stage Definition

The following simulations present a sequence of empirical clinical simulations of abdominal aortic aneurysm progression, implemented in Python through the three-dimensional Lattice Boltzmann framework introduced in Section 2. The flow field was computed from the discretized Boltzmann formulation and interpreted together with the wall-stress relation associated with aneurysmal enlargement, allowing the generation of three-dimensional visualizations of the aorta under progressive pathological conditions [13, 14, 17, 18]. The simulated sequence was organized into six principal stages: healthy aorta, initial dilation, mild aneurysm, moderate aneurysm, advanced aneurysm, and rupture. These stages were defined from representative geometric, hemodynamic, and biomechanical values reported in the literature [15, 16, 19, 20].

Table 6 summarizes the clinical and mathematical reference values used to organize the progression shown in the following figures. From a physical and bioengineering perspective, the increase in vessel diameter raises the circumferential stress supported by the aortic wall, while progressive wall thinning reduces the structural capacity of the vessel to withstand internal blood pressure [17, 18]. This combined effect explains why advanced aneurysmal stages are associated with greater instability and higher rupture risk.

4.8.2 Simulation 1: Global Evolution of Abdominal Aortic Aneurysm

Figure 6 presents the complete six-stage evolution from the healthy aorta to rupture, together with local wall views highlighting progressive weakening. This figure was generated from the stage sequence defined in Table 6, using the three-dimensional simulated geometry as the basis for visual interpretation [17, 18].

This image provides a clinically intuitive view of aneurysm progression. In Stages 1 and 2, the vessel remains mostly stable, although early geometric alteration is already visible. In Stages 3 to 5, the aneurysmal sac enlarges and the wall becomes progressively weaker, which is represented by the change in color intensity. Stage 6 corresponds to rupture, when the wall can no longer sustain the imposed mechanical load. The lower insets reinforce this interpretation by showing the local transition from a healthy wall to thinning, critical weakening, and rupture. Physically, the figure illustrates that aneurysm progression is not only a geometric problem, but also a biomechanical process involving loss of wall strength under continued hemodynamic loading [17, 20].

4.8.3 Simulation 2: Progressive Loss of Aortic Wall Elasticity

Figure 7 emphasizes the mechanical response of the aortic wall during aneurysm progression. The visualization focuses on the gradual loss of elasticity, from the normal condition to stretching and finally rupture. The color bar indicates the relative increase in mechanical demand over the aneurysmal region [17, 18].

In this figure, the wall behavior is interpreted in terms of elastic response. The first configuration represents the normal vessel, in which the wall can accommodate physiological pressure. The intermediate configurations labeled as stretching represent progressive deformation of the aneurysmal segment, where the wall still carries the load but under increasing stress. The last configuration represents rupture, indicating that the structural resistance has been exceeded. This figure contains **seven** aortic shapes, whereas the other figures use **six** main stages, because here an additional transitional stretching state was included to illustrate the mechanical evolution more gradually before final wall failure. This extra

Table 6. Representative parameters adopted for the six simulated stages of abdominal aortic aneurysm progression, based on published data [15–20].

Stage	Clinical condition	Diameter (mm)	Pressure (mmHg)	Wall thickness (mm)	Structural interpretation
1	Healthy aorta	17.5–20	120/80	2.0–2.2	Physiological condition
2	Initial dilation	25–29	125/82	2.0	Early geometric alteration
3	Mild aneurysm	30–39	130/85	1.9–2.0	Localized dilation with moderate weakening
4	Moderate aneurysm	40–49	140/90	1.8–1.9	Increased wall loading
5	Advanced aneurysm	50–55	160/95	1.6–1.8	High-risk biomechanical state
6	Rupture / failure stage	60–65	180/110	1.5–1.7	Loss of wall integrity

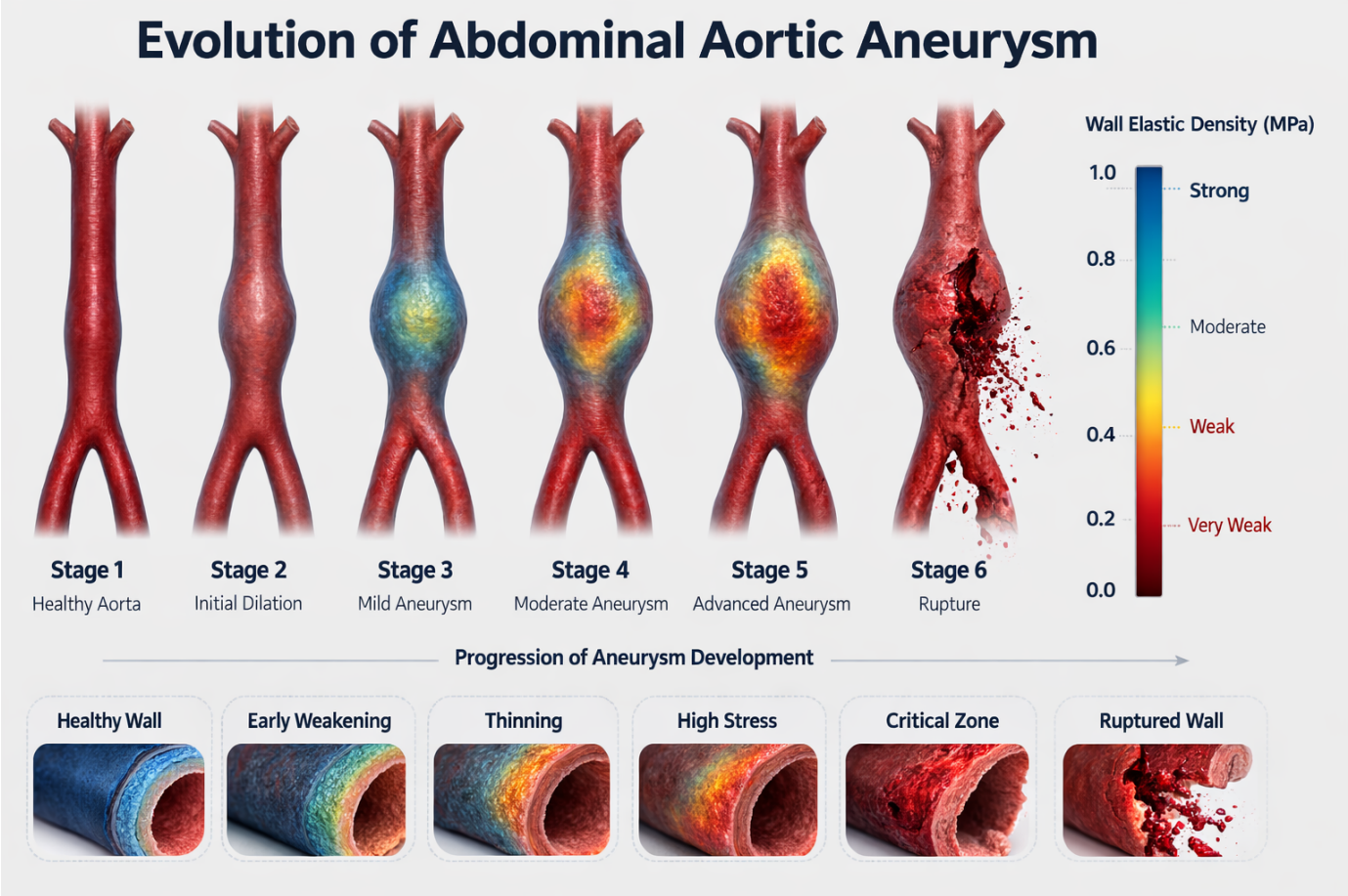

Figure 6. Progressive six-stage simulation of abdominal aortic aneurysm evolution, from healthy geometry to rupture.

step is useful from a biomechanical perspective because wall weakening is progressive rather than instantaneous [18, 20].

4.8.4 Simulation 3: Stage-by-Stage Hemodynamic Loading

Figure 8 presents six successive stages with color-coded hemodynamic loading. The purpose of this simulation is to show how the internal mechanical demand grows as the aneurysm enlarges. The stage numbering follows the same progression defined in Table 6 [15, 18, 19].

The first two stages are associated with relatively stable loading conditions. Beginning with Stage 3, the aneurysmal region starts to accumulate higher mechanical demand, which becomes more evident in Stages 4 and 5. By Stage 6, the vessel is already in

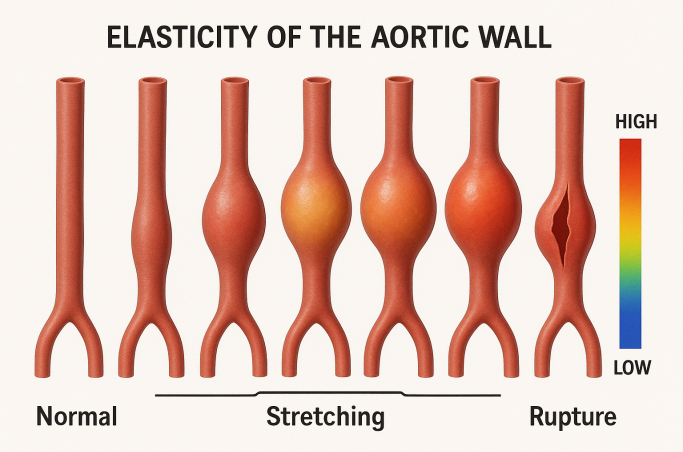

Figure 7. Simulation of the progressive loss of aortic wall elasticity from the normal state to rupture.

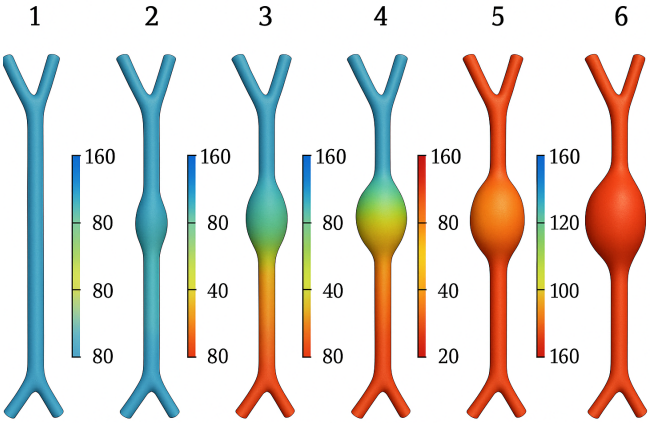

Figure 8. Six-stage simulation of hemodynamic loading during aneurysm progression.

a severely compromised condition. Physically, this progression indicates that the aneurysm changes the distribution of internal pressure and stress along the wall. From the viewpoint of applied mathematics and bioengineering, the figure shows how a gradual change in geometry may produce a strongly nonlinear increase in local mechanical burden [17, 18].

4.8.5 Simulation 4: Wall Elasticity Field During Aneurysm Evolution

Figure 9 presents the evolution of a wall-elasticity field over six progressive stages. In this representation, the color scale is used to describe the transition from preserved mechanical response to severe local weakening, with rupture appearing in the final step [18, 20].

This figure highlights that aneurysm growth is accompanied by loss of mechanical homogeneity. In the initial stages, the wall response remains relatively uniform. As the aneurysm expands, a

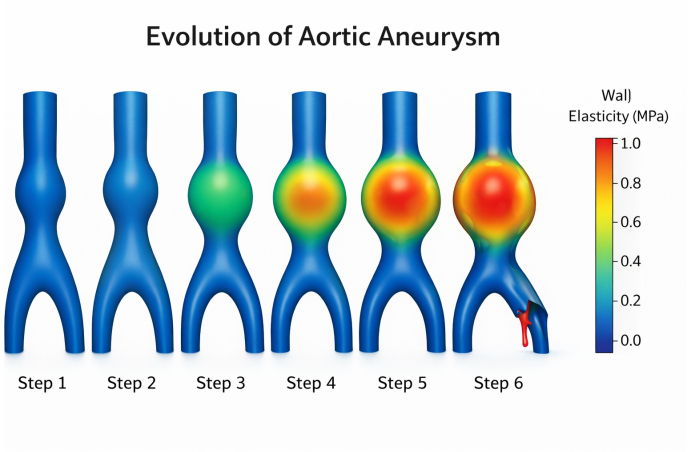

Figure 9. Six-stage simulation of wall elasticity evolution in the abdominal aorta.

concentrated critical zone develops in the enlarged region, indicating that the wall no longer distributes the load evenly. In the last stage, rupture occurs at the structurally weakest site. Clinically, this means that the aneurysm does not fail everywhere simultaneously; instead, failure tends to occur in the region where weakening, stress concentration, and geometric enlargement interact most strongly [17, 18].

4.8.6 Simulation 5: Pure Geometric Evolution of the Aneurysm

Figure 10 isolates the geometric progression of the aneurysm without additional field coloring. This representation is useful because it shows the structural sequence in a simplified form, allowing direct comparison between the healthy vessel, the onset of dilation, the intermediate aneurysmal stages, and the final ruptured geometry [15, 16].

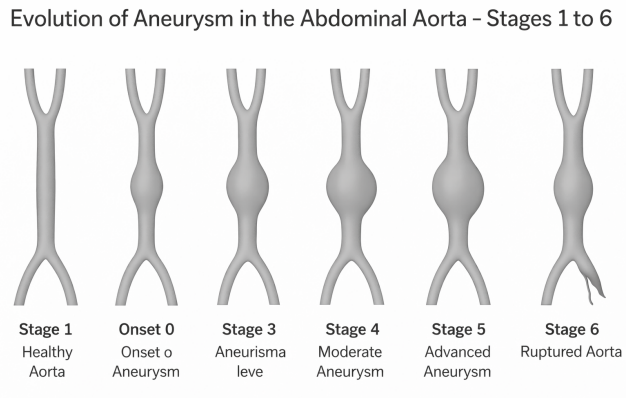

Figure 10. Pure geometric evolution of the abdominal aortic aneurysm from the healthy state to rupture.

From a physical perspective, this figure shows that aneurysm progression begins with a small local dilation, evolves through gradual enlargement of the

sac, and culminates in structural failure. Because no additional hemodynamic field is superimposed, the reader can focus on the morphological evolution alone. This is important in cardiovascular bioengineering, since geometry is one of the main determinants of pressure redistribution, wall stress concentration, and rupture risk [15, 17].

4.9 General Interpretation of the Simulated Sequence

Taken together, Figures 6–10 provide complementary views of the same pathological process. Some emphasize global morphology, others emphasize wall elasticity, and others highlight the stage-by-stage increase in mechanical loading. The common interpretation is that abdominal aortic aneurysm progression is governed by the combined effect of geometry, pressure loading, wall thinning, and loss of structural resistance [16–18]. Thus, the sequence of simulations supports the clinical and mathematical idea that rupture is the final consequence of progressive biomechanical instability rather than an isolated event.

5 Conclusion

This study presented a mathematical and computational analysis of blood flow in the abdominal aorta under healthy, aneurysmal, and rupture-related conditions. Based on the Newtonian constitutive relation in Eq. (5) and on the Lattice Boltzmann formulation introduced in the mathematical modeling section, a numerical framework was implemented in Python to simulate the hemodynamic behavior of the abdominal aorta and to generate three-dimensional visual representations of its pathological evolution. In the present work, blood was modeled as an incompressible Newtonian fluid, which is a suitable approximation for large arteries such as the abdominal aorta.

The numerical results showed a clear transition from physiological flow conditions in the healthy aorta to increasingly disturbed hemodynamics in the aneurysmal and rupture-related stages. As the vessel diameter increased, the simulations indicated significant changes in velocity distribution, pressure loading, and wall shear stress, particularly in the dilated region. These results are physically consistent with the expected biomechanical behavior of abdominal aortic aneurysms, since geometric enlargement increases local wall stress and reduces the structural stability of the vessel wall.

The rupture-related simulations highlighted the progressive transition from mechanically stable conditions to critical wall failure. In the advanced stages, the concentration of hemodynamic loading in the aneurysmal sac became more pronounced, indicating progressive weakening of the wall and greater rupture susceptibility. From a clinical perspective, this result is relevant because it helps explain how aneurysm growth may evolve toward rupture under adverse pressure and structural conditions. Thus, the proposed model contributes not only to the mathematical description of the problem, but also to the physical and biomechanical interpretation of aneurysm progression.

The novelty of the present research lies in the integration of a mathematically grounded Lattice Boltzmann approach, a three-dimensional representation of abdominal aortic aneurysm progression, and a clinically interpretable analysis of pressure-related wall loading and rupture risk within a single computational framework. Unlike a purely theoretical or purely visual analysis, the present study connects fluid mechanics, numerical simulation, and bioengineering interpretation in a way that helps bridge the gap between mathematical modeling and clinically meaningful vascular assessment.

Therefore, this work has innovative potential in the medical field because it provides a computationally interpretable framework for studying aneurysm development, wall weakening, and rupture-related behavior. In addition, the study contributes to the advancement of bioengineering, biomathematics, and cardiovascular modeling by combining numerical methods, vascular geometry, and physical interpretation of the results. For these reasons, the proposed framework may support future developments in diagnostic assistance, rupture-risk analysis, and personalized approaches in vascular medicine.

Data Availability Statement

Data will be made available on request.

Funding

This work was supported without any funding.

Conflicts of Interest

The authors declare no conflicts of interest.

AI Use Statement

The authors declare that no generative AI was used in the preparation of this manuscript.

Ethical Approval and Consent to Participate

This study did not involve human participants, animal subjects, or any clinical data. Therefore, ethical approval and consent to participate were not required.

References

[1] Haque, K., & Bhargava, P. (2022). Abdominal aortic aneurysm. *American family physician, 106*(2), 165-172.

[2] Lindquist Liljeqvist, M., Bogdanovic, M., Siika, A., Gasser, T. C., Hultgren, R., & Roy, J. (2021). Geometric and biomechanical modeling aided by machine learning improves the prediction of growth and rupture of small abdominal aortic aneurysms. *Scientific Reports, 11*(1), 18040. [CrossRef]

[3] Wang, X., Ghayesh, M. H., Kotousov, A., Zander, A. C., Amabili, M., Dawson, J. A., & Psaltis, P. J. (2023). Biomechanics of abdominal aortic aneurysm in the framework of Windkessel effect and fully-developed inflow velocity via two-way non-linear FSI. *International Journal of Non-Linear Mechanics, 157*, 104517. [CrossRef]

[4] Yue, X., Huang, J., & Liu, J. (2025). Fluid-structure interaction analysis for abdominal aortic aneurysms: the role of multi-layered tissue architecture and intraluminal thrombus. *Frontiers in Bioengineering and Biotechnology, 13*, 1519608. [CrossRef]

[5] Aydin, F. M., & Yalcin, H. C. (2025). Modeling Techniques and Boundary Conditions in Abdominal Aortic Aneurysm Analysis: Latest Developments in Simulation and Integration of Machine Learning and Data-Driven Approaches. *Bioengineering, 12*(5), 437. [CrossRef]

[6] Rezaeitaleshmahalleh, M., Lyu, Z., Mu, N., Zhang, X., Rasmussen, T. E., McBane, R. D., & Jiang, J. (2023). Characterization of small abdominal aortic aneurysms' growth status using spatial pattern analysis of aneurismal hemodynamics. *Scientific reports, 13*(1), 13832. [CrossRef]

[7] Kalender, G., Weissmann, T., & Dinç, U. (2024). A Decade-Long Retrospective Study of Factors Influencing Survival in Ruptured Abdominal Aortic Aneurysm. *Journal of Clinical Medicine, 13*(21), 6431. [CrossRef]

[8] Meuli, L., Zimmermann, A., Petersen, J. K., Fosbøl, E. L., Dabravolskaité, V., Makaloski, V., ... & Resch, T. A. (2025). Risk stratification and treatment selection in patients with asymptomatic abdominal aortic aneurysms. *JAMA network open, 8*(4), e253559. [CrossRef]

[9] Wang, L., Dong, D., & Tian, F. B. (2022). Fast prediction of blood flow in stenosed arteries using machine learning and immersed boundary-lattice Boltzmann method. *Frontiers in physiology, 13*, 953702. [CrossRef]

[10] Shen, Y., Wei, Y., Bokkers, R. P. H., Uyttenboogaart, M., & van Dijk, M. C. (2022). Patient-Specific Cerebral Blood Flow Simulation Based on Commonly Available Clinical Datasets. *Frontiers in Bioengineering and Biotechnology, 10*, 835347. [CrossRef]

[11] Yei, K., Mathlouthi, A., Naazie, I., Elsayed, N., Clary, B., & Malas, M. (2022). Long-term Outcomes Associated With Open vs Endovascular Abdominal Aortic Aneurysm Repair in a Medicare-Matched Database. *JAMA Network Open, 5*(5), e2212081. [CrossRef]

[12] Myneni, M., & Rajagopal, K. R. (2022). Constitutive modeling of the mechanical response of arterial tissues. *Applications in Engineering Science, 11*, 100111. [CrossRef]

[13] Fuchs, A., Berg, N., Fuchs, L., & Prahl Wittberg, L. (2023). Assessment of rheological models applied to blood flow in human thoracic aorta. *Bioengineering, 10*(11), 1240. [CrossRef]

[14] Zhu, Y., Li, F., Zhang, H., Song, H., Ma, X., Cao, L., ... & Guo, W. (2022). Hemodynamic numerical simulation of aortic arch modular inner branched stent-graft in eight early patients from the first-in-human case series. *Frontiers in Cardiovascular Medicine, 9*, 981546. [CrossRef]

[15] Kim, H., Kwon, T. W., Choi, E., Jeong, S., Kim, H. K., Han, Y., ... & Kim, W. H. (2022). Aortoiliac diameter and length in a healthy cohort. *PLoS One, 17*(5), e0268077. [CrossRef]

[16] Golledge, J., Thanigaimani, S., Powell, J. T., & Tsao, P. S. (2023). Pathogenesis and management of abdominal aortic aneurysm. *European heart journal, 44*(29), 2682-2697. [CrossRef]

[17] McGloughlin, T. M., & Doyle, B. J. (2010). New approaches to abdominal aortic aneurysm rupture risk assessment: engineering insights with clinical gain. *Arteriosclerosis, thrombosis, and vascular biology, 30*(9), 1687-1694. [CrossRef]

[18] Che, Y., Cao, X., Cao, Z., Zhang, Y., Zhu, J., Shu, C., ... & Zhang, X. (2025). Rupture prediction of medium to large-sized abdominal aortic aneurysm combining wall shear stress-related parameters and anatomical characteristics: A computational, experimental, and statistical analysis. *Physics of Fluids, 37*(1). [CrossRef]

[19] Columbo, J. A., Scali, S. T., Jacobs, B. N., Scully, R. E., Suckow, B. D., Huber, T. S., ... & Stone, D. H. (2024). Size thresholds for repair of abdominal aortic aneurysms warrant reconsideration. *Journal of vascular*

surgery, 79(5), 1069-1078. [CrossRef]

[20] Fasen, F., van der Horst, A., van Sambeek, M. R., & Lopata, R. G. (2025). In vivo regional wall thickness measurement of abdominal aortic aneurysms using intravascular ultrasound. *JVS-Vascular Insights*, 100297. [CrossRef]

[21] Hao, W., Gong, S., Wu, S., Xu, J., Go, M. R., Friedman, A., & Zhu, D. (2017). A mathematical model of aortic aneurysm formation. *PloS one, 12*(2), e0170807. [CrossRef]

[22] Rüttgers, M., Waldmann, M., Ito, S., Wüstenhagen, C., Grundmann, S., Brede, M., & Lintermann, A. (2025). Patient-specific lattice-Boltzmann simulations with inflow conditions from magnetic resonance velocimetry measurements for analyzing cerebral aneurysms. *Computers in biology and medicine, 187*, 109794. [CrossRef]

[23] Owen, B., Lowe, C., Ashton, N., Mandal, P., Rogers, S., Wein, W., ... & Revell, A. (2016). Computational hemodynamics of abdominal aortic aneurysms: three-dimensional ultrasound versus computed tomography. *Proceedings of the Institution of Mechanical Engineers, Part H: Journal of Engineering in Medicine, 230*(3), 201-210. [CrossRef]

[24] Stergiou, Y. G., Kanaris, A. G., Mouza, A. A., & Paras, S. V. (2019). Fluid-Structure Interaction in Abdominal Aortic Aneurysms: Effect of Haematocrit. *Fluids, 4*(1), 11. [CrossRef]

[25] Nicolajsen, C. W., Søgaard, M., Jensen, M., Eldrup, N., Larsen, T. B., Goldhaber, S. Z., ... & Nielsen, P. B. (2023). Antiplatelet therapy in patients with abdominal aortic aneurysm without symptomatic atherosclerotic disease. *JAMA network open, 6*(10), e2339715. [CrossRef]

[26] Kim, D., Narayanan, D., Sung, S. H., Cheng, H. M., Chen, C. H., Kim, C. S., ... & Hahn, J. O. (2024). Transmission line model as a digital twin for abdominal aortic aneurysm patients. *NPJ Digital Medicine, 7*(1), 301. [CrossRef]

[27] Liang, L., Liu, M., Martin, C., Elefteriades, J. A., & Sun, W. (2017). A machine learning approach to investigate the relationship between shape features and numerically predicted risk of ascending aortic aneurysm. *Biomechanics and modeling in mechanobiology, 16*(5), 1519-1533. [CrossRef]

[28] Scotti, C. M., Shkolnik, A. D., Muluk, S. C., & Finol, E. A. (2005). Fluid-structure interaction in abdominal aortic aneurysms: effects of asymmetry and wall thickness. *Biomedical engineering online, 4*(1), 64. [CrossRef]

[29] Olaoluwa Omole, E., Olusheye Adeyefa, E., Iyabo Apanpa, K., Iyadunni Ayodele, V., Emmanuel Amoyedo, F., & Emadifar, H. (2024). Unveiling the Power of Implicit Six-Point Block Scheme: Advancing numerical approximation of two-dimensional PDEs in physical systems. *Plos one, 19*(5), e0301505. [CrossRef]

Matheus dos Santos Farias holds a bachelor's degree in Physics from the University of São Paulo (USP) and a teaching degree in Pedagogy. He also completed postgraduate studies at the Albert Einstein Israelite Hospital. Currently, he is pursuing a master's degree in Nuclear Physics at the Institute for Nuclear and Energy Research (IPEN). This article is one of the research projects developed during my undergraduate studies in physics, and I am pleased to submit one of my works for publication in this journal. (Email: matheusfariasfm@gmail.com)